Biomaterials Advances 160 (2024) 213849

Contents lists available at ScienceDirect

Biomaterials Advances

journal homepage: www.journals.elsevier.com/materials-science-and-engineering-c

# "A lactose-modified chitosan accelerates chondrogenic differentiation in mesenchymal stem cells spheroids"

F. Scognamiglio [a,*], C. Pizzolitto [b], M. Romano [c], G. Teti [d], S. Zara [e], M. Conz [a], I. Donati [a], D. Porrelli [b,1], M. Falconi [f], E. Marsich [b]

[a] Department of Life Sciences, University of Trieste, Via Licio Giorgieri 5, 34127 Trieste, Italy
[b] Department of Medicine, Surgery and Health Sciences, University of Trieste, Piazza dell'Ospitale 1, 34129 Trieste, Italy
[c] Department of Life Sciences, University of Trieste, Via Valerio 28, 34127 Trieste, Italy
[d] Department of Biomedical and Neuromotor Sciences, University of Bologna, Via Irnerio 48, 40126 Bologna, Italy
[e] Department of Pharmacy, University "G. d'Annunzio" Chieti-Pescara, Via dei Vestini 31, 66100 Chieti, Italy
[f] Department of Medical and Surgical Sciences, University of Bologna, Via Irnerio 48, 40126 Bologna, Italy

ARTICLE INFO

*Keywords:*
Spheroids
Lactose-modified chitosan
Cartilage
Mesenchymal stem cells
Collagen

ABSTRACT

Spheroids derived from human mesenchymal stem cells (hMSCs) are of limited use for cartilage regeneration, as the viability of the cells progressively decreases during the period required for chondrogenic differentiation (21 days). In this work, spheroids based on hMSCs and a lactose-modified chitosan (CTL) were formed by seeding cells onto an air-dried coating of CTL. The polymer coating can inhibit cell adhesion and it is simultaneously incorporated into spheroid structure. CTL-spheroids were characterized from a morphological and biological perspective, and their properties were compared with those of spheroids obtained by seeding the cells onto a non-adherent surface (agar gel). Compared to the latter, smaller and more viable spheroids form in the presence of CTL as early as 4 days of culture. At this time point, analysis of stem cells differentiation in spheroids showed a remarkable increase in collagen type-2 (COL2A1) gene expression (~700-fold compared to day 0), whereas only a 2-fold increase was observed in the control spheroids at day 21. These results were confirmed by histological and transmission electron microscopy (TEM) analyses, which showed that in CTL-spheroids an early deposition of collagen with a banding structure already occurred at day 7. Overall, these results support the use of CTL-spheroids as a novel system for cartilage regeneration, characterized by increased cell viability and differentiation capacity within a short time-frame. This will pave the way for approaches aimed at increasing the success rate of procedures and reducing the time required for tissue regeneration.

## 1. Introduction

Articular cartilage is a connective tissue devoid of nerves, blood and lymphatic vessels, composed by a single cell population (chondrocytes) that is embedded in an extracellular matrix (ECM) mainly composed of collagen fibers and glycosaminoglycans (GAGs). Mechanical trauma, aging or inflammatory diseases can affect both the structure and functions of articular cartilage, that has a limited self-repair capacity due to the absence of blood vessels and to the low replicative ability of chondrocytes [1,2].

Nowadays, damaged cartilage can be regenerated either by surgical approaches (microfractures, Autologous Chondrocyte Implantation - ACI, Matrix-Associated Autologous Chondrocyte Implantation – MACI, Autologous Matrix-Induced Chondrogenesis - AMIC) or by cell therapies based on chondrocytes or mesenchymal stem cells (MSCs) [2–4].

Chondrocytes can be harvested from a patient's biopsy, but their use is limited since they can undergo de-differentiation when cultured in vitro. Instead, MSCs are optimal candidates for cell therapy, as they are easily available, have high differentiation and proliferation potential, and display anti-inflammatory and immunomodulatory properties [3,5]. Further improvement in cartilage regeneration has recently been achieved with spheroids [6,7].

* Corresponding author at: University of Trieste – Department of Life Sciences, Via Licio Giorgieri, 5, 34127 Trieste, Italy.
*E-mail addresses:* fscognamiglio@units.it (F. Scognamiglio), CHIARA.PIZZOLITTO@phd.units.it (C. Pizzolitto), mromano@units.it (M. Romano), gabriella.teti2@unibo.it (G. Teti), s.zara@unich.it (S. Zara), MARCO.CONZ@studenti.units.it (M. Conz), idonati@units.it (I. Donati), dporrelli@units.it (D. Porrelli), mirella.falconi@unibo.it (M. Falconi), emarsich@units.it (E. Marsich).
[1] **Present address:** Department of Life Sciences, University of Trieste, Via Alexander Fleming 31/B, 34127-Trieste, Italy.

https://doi.org/10.1016/j.bioadv.2024.213849
Received 6 October 2023; Received in revised form 27 March 2024; Accepted 3 April 2024
Available online 4 April 2024

Spheroids are 3D cell structures with self-assembly capacities that reproduce the environment in vivo with higher similarity than 2D cell cultures. As to the cell source, MSCs from adipose tissue cultured in the form of spheroids display the highest chondrogenic potential compared to stem cells derived from dental pulp and Wharton's jelly [8].

The main advantage of spheroids over 2D cell cultures is the maintenance of cell-cell and cell-matrix interactions, which occurs through the interaction with membrane integrins and cadherins [9–11].

Spheroids can be prepared through various techniques [12]. Among them, preventing cell adhesion to tissue culture plates is a simple, fast and inexpensive strategy [12–16].

This approach has recently been employed to prepare hybrid cell-polymer aggregates as a novel cell-based therapy for the treatment of cartilage defects [17]. These cellular aggregates (named chondro-aggregates) consist in a two-components systems composed of chondrocytes and of a lactose-modified chitosan (namely, CTL), whose bioactivity has been demonstrated in terms of stimulating the synthesis of the cartilage matrix components in primary chondrocytes [18], acting as a scavenger for Reactive Oxygen Species (ROS) [19] and, in combination with hyaluronic acid (HA), reducing inflammation and oxidative stress [20] and stimulating the synthesis of collagen type-2 and GAGs in chondrocyte-based nodules [21]. Moreover, biomaterials in the form of hydrogels and membranes based on this polymer have been developed for cartilage and osteo-articular applications [19,22].

Despite the high regenerative potential of spheroids, the aggregation of cells leads to compact structure with close cell-cell interactions, which prevents the diffusion of oxygen and nutrients. The depletion of these elements causes the necrosis of cells in the central region (necrotic core) with a general reduction of spheroids viability, limiting their use for tissue engineering (TE) applications.

Starting from these observations, in this work we propose a strategy based on the use of the polymer CTL combined with mesenchymal stem cells (MSCs) to form 3D spheroids (namely CTL-spheroids) for applications in cartilage regeneration.

In CTL-spheroids the polymer CTL formed a matrix that was integrated in the structure of the spheroids, and thus eliciting biological responses related to chondrogenic differentiation. To elucidate the role of the CTL matrix in leading to these biological responses, spheroids without matrices (namely matrix-free spheroids – MF-spheroids) consisting only of cells were selected.

The presence of CTL in spheroids delays the formation of large aggregates at early time points, thus improving their overall viability. In these spheroids, the process of chondrogenic differentiation was accelerated compared to MF-spheroids, as confirmed by gene and protein expression analyses. These results were confirmed by histological and ultrastructural analyses, pointing out the increased deposition of mature collagen-type 2 in CTL-spheroids.

Overall, compared to conventional clinical approaches for cartilage regeneration, the incorporation of CTL in MSCs-spheroids appears to be a novel strategy that has the advantage of favoring the formation of smaller and more viable 3D structures, in which chondrogenic differentiation is accelerated.

## 2. Materials and methods

### 2.1. Materials

Lactose-modified chitosan in hydrochloride form, CTL (CAS Registry Number 2173421.37–7), with fractions of *N*-acetyl-glucosamine (GlcNAc; "acetylated", A) ($F_A$) = 0.16; glucosamine ($GlcNH_2$; "deacetylated", D) ($F_D$) = 0.21; and lactitol substituted D unit (N-alkylated GlcLac; "lactitol", L) ($F_L$) = 0.63, was kindly provided by Biopolife S.r.L. (Trieste, Italy). The intrinsic viscosity [η] was 344 mL/g, determined at 25 °C by viscosimetry (CT1150 Schott Geräte automatic measuring apparatus and a Schott capillary viscometer), and the estimated molecular weight was 780,000 g/mol [23]. Agar was kindly provided by Java Biocolloid Europe Srl.

Phosphate-buffered saline (PBS), Triton X-100, sodium hydroxide (NaOH), formaldehyde 40 % *w/v*, bovine serum albumin (BSA), poly (vinyl alcohol), (MOWIOL 4–88), normal goat serum (NGS), Trizol, Fluorescein isothiocyanate (FITC), Human Mesenchymal Stem Cells derived from adipose tissue, Transforming growth factor-β1 (TGF-β1), dexamethasone, Live/Dead assay kit, hexamethyldisilazane (HMDS), Alamar Blue were all purchased from Sigma-Aldrich. Insulin-Transferrin-Selenium-Sodium Pyruvate (ITS-A) was from Gibco™. Ethanol was purchased from Carlo Erba. L-Ascorbic acid was from Fluka Biochemika. Mesenchymal Stem Cell Growth Medium 2 was from PromoCell. Penicillin/streptomycin, trypsin-ethylenediaminetetraacetic acid (EDTA) 1× and fetal bovine serum (FBS) were purchased from EuroClone s.p.a. Collagen II monoclonal antibody (catalog number #MA5-12789) and Goat anti-Mouse IgG (H + L) Highly Cross-Adsorbed Secondary Antibody, Alexa Fluor™ 594 (catalog number #A-11032), M-MLV reverse transcriptase and microBCA assay were from Thermo Fisher Scientific. Hoechst 33258 was from Invitrogen (Bleiswijk, The Netherlands). Paraffin, Bio-Clear solvent, Hematoxylin Mayer's solution, Eosin solution and Masson Trichrome kit were all purchased from Bio-Optica (Milan, Italy). Glutaraldehyde and osmium tetroxide ($OsO_4$) solutions were respectively purchased from Sigma Aldrich and Società Italiana Chimici. Human CTXII ELISA Kit was from FineTest.

### 2.2. Preparation of CTL-spheroids and MF-spheroids

CTL-spheroids and MF-spheroids were prepared according to protocols already reported in the literature [17,21], with slight modifications. To prepare CTL-spheroids, a CTL solution was prepared in PBS 1× (2 % *w/v*) and the pH was set at 7.4. This solution (400 μL) was employed to coat the wells of 24-well plate and air-drying was allowed overnight. The wells were then sterilized by UV-rays for 20 min. Human Mesenchymal Stem Cells derived from adipose tissue (hMSCs-AT) were cultured in cell medium supplemented with penicillin/streptomycin 1 % and supplementary mix 10 %, according to manufacturer's instructions. At the day of seeding (time zero), the cells were trypsinized and 60,000 cells were plated in each well, in 1.5 mL of chondrogenic medium (ascorbic acid 100 μM, dexamethasone 0.1 μM, Transforming Growth Factor-β - TGF-β - 10 ng/mL, Insulin-Transferrin-Selenium-Sodium Pyruvate – ITS-A 1×). Matrix-free spheroids (MF-spheroids) were prepared by seeding hMSCs-AT at the same cell density in chondrogenic medium, but the wells were coated with an agar gel (2 % *w/v* in PBS 1×) to prevent cell adhesion. The cells were cultured in chondrogenic medium up to 21 days. Once a week 700 μL of medium were removed from each well and fresh chondrogenic medium was added (800 μL).

### 2.3. Analysis of spheroid dimensions

The analysis of spheroids dimension was evaluated using an optical microscope (Optech IB3 ICS) equipped with a Pentax K100D camera, using 4× as objective. This analysis was performed only for those time points at which spheroids could be still recognized as single entities (i.e. day 1, day 4 and day 7 for CTL-spheroids; day 1 and day 4 for MF-spheroids), by using the Fiji-ImageJ software. For these time point, the pictures were acquired and the diameter of spheroids was calculated. Data were averaged and standard deviation calculated.

### 2.4. Cell viability assay (Alamar Blue)

The viability of spheroids was evaluated by the Alamar Blue assay. CTL and MF-spheroids were collected at day 1, 4, 7, 11 and 14 of culture, transferred to an Eppendorf tube and centrifuged at 69 *g* for 5 min. Alamar Blue was added to complete cell medium (dilution 1:30) and 300 μL of this solution were added to each sample. Incubation was allowed for 4 h, at 37 °C in the dark. The medium (200 μL) was transferred to a plate and fluorescence intensity was read with a fluorimeter

FLUOStar Omega-BMG Labtech spectrophotometer (excitation: 544 nm; emission: 590 nm). For each time point, four replicates were averaged and standard deviation calculated. Statistical analysis was performed by an unpaired Student *t*-test ($p$-value $<0.05$ was considered as statistical significant).

### 2.5. Live/dead assay

The viability of the spheroids was analyzed qualitatively using a Live/Dead assay kit. Spheroids samples were cultured for 1, 4, 7 and 14 days. At each time point, 2 μL of solution A (containing calcein-AM) and 1 μL of solution B (containing propidium iodide) were added to 1 mL of PBS 1×. Then, 100 μL of the resulting mixture were added to the sample. Images were captured using a Nikon Eclipse Ti-E epifluorescence live-imaging microscope.

### 2.6. Scanning Electron Microscopy (SEM)

The morphology of spheroids was investigated by Scanning Electron Microscopy (SEM) analyses. Spheroids samples were collected at day 4, 7 and 14. At these time points the spheroids were collected, washed with PBS 1× and fixed with glutaraldehyde 2.5 % in PBS 1× for 1 h at room temperature (RT). The fixative was then removed and the samples were washed with PBS 1×, gradually dehydrated in ethanol (30 %, 70 %, 100 % *v*/v in deionized water), then substituted by hexamethyldisilazane (HMDS, 30 %, 70 % 100 % v/v in ethanol), which was air-dried at room temperature. Each of these step was performed for 20 min at RT. For SEM analyses the spheroid samples were placed on aluminum stubs covered with a double-sided carbon tape and sputter-coated with gold using a Sputter Coater K550X (Emitech, Quorum Technologies Ltd., U. K.). The analyses were performed using a scanning electron microscope (Quanta 250 SEM, FEI, Oregon), working in secondary electron detection mode. The acceleration voltage was set at 30 kV, while the working distance was set at 10 mm.

### 2.7. Synthesis of CTL labelled with fluorescein isothiocyanate

To label CTL with fluorescein isothiocyanate (FITC), CTL (500 mg) was dissolved in deionized water (167 mL) under stirring, and FITC solution (1.1 mL; 0.5 mg/mL in sodium bicarbonate buffer 50 mM) was added to the CTL solution. The incubation was allowed for 24 h in dark, at room temperature (RT). This solution was then dialyzed (Spectrapore, MWCO 12′000) against $NaHCO_3$ 50 mM, NaCl 100 mM and against water until the conductance was lower than 3 μS/cm at 4 °C. The pH of the solution was set at 4.5 and freeze-dried using an ALPHA 1–2 LD plus freeze-dryer (CHRIST, Osterode am Harz, Germany).

### 2.8. Localization of CTL in CTL-spheroids

The analysis of CTL localization in CTL-spheroids was performed following a protocol already described in Pizzolitto et al. [17]. The CTL solution employed for the coating of the well contained CTL and fluorescent-labelled CTL in ratio 1:1. CTL-spheroids were collected at day 4, 7 and 14, washed in PBS 1× and fixed in formaldehyde 4 % *v*/v in PBS 1× for 15 min at room temperature. The samples were then washed 3 times in PBS 1× and incubated with Triton 0.2 % v/v in PBS 1× for 15 min at room temperature. The spheroids were washed in PBS 1× and incubated with the blocking solution containing Bovine Serum Albumin (BSA) 4 % *w/v* and Normal Goat Serum (NGS) 5 % v/v in PBS 1×, for 1 h at 37 °C. The blocking solution was then removed, the spheroids were washed with PBS 1× and treated with Hoechst (diluted 1:1000 in PBS 1×) for 10 min at RT to visualize cell nuclei. The spheroids were washed with PBS and visualized by a Nikon Eclipse Ti-E epifluorescence live-imaging microscope.

### 2.9. Light microscopy analyses on spheroids

Spheroids samples were collected at day 4, 7 and 14, washed with PBS 1× and fixed with paraformaldehyde 4 % *w/v* in PBS 1× for 20 min at RT. The fixative was removed and a washing step was performed twice in PBS 1×. The spheroids were then included in an agarose gel. For the inclusion step, agarose was dissolved in PBS 1× (1.5 % *w/v*) by using a microwave and cooled down at 37 °C. This solution (100 μL) was added to the spheroid pellet and rapidly transferred to a circular mold. The agarose gel containing the spheroid was then employed for the light microscopy analyses. Subsequently, samples were dehydrated through ascending alcohols series, and then paraffin embedded. Next, samples were dewaxed (alcohols at progressively decreasing concentrations) and cut, by means of a rotary microtome, in sections 4 μm thick; sections were further processed for Hematoxylin-Eosin (H/E) and Masson's Trichrome stainings. After that, randomly selected sections for each experimental point were observed and acquired by Leica DM 4000 light microscope (Leica Cambridge Ltd., Cambridge, UK) equipped with a Leica DFC 320 camera (Leica Cambridge Ltd., Cambridge, UK). Leica Application Suite X (LASX) (Leica Cambridge Ltd., Cambridge, UK) image analysis software was employed for the acquisition of images.

### 2.10. Real time PCR on spheroids

Spheroids samples were collected by centrifugation (69 *g* for 5 min) at day 4, 7 and 14 and washed twice with PBS 1×. The spheroid pellet was resuspended in PBS 1× (200 μL), Triton X-100 (800 μL) was added to each sample. The samples were stored at −20 °C overnight for RNA extraction. Total RNA was purified from cells by using Trizol, according to manufacturer's protocol. For cDNA synthesis, 500 ng of RNA were retrotranscribed with M-MLV reverse transcriptase (Thermo Fisher Scientific, Waltham, MA, USA) and hexameric random primers. Gene expression levels of genes of interest were determined by quantitative Real Time PCR (qPCR) by using a CFX96 Real-Time PCR detection system (Bio-Rad Laboratories, Redmond, WA, USA) and SYBR Green methodology (Bio-Rad Laboratories, Redmond, WA, USA). The primer pair used to analyze gene expression levels of genes of interest (5 to 3′) are reported in Table 1:

The expression of the house-keeping genes GAPDH was used to normalize targets' gene expression, and the relative expression levels were calculated using the 2^-ΔΔCT method [24].

The results are representative of two independent experiments in triplicate. Statistical significance was calculated by unpaired T-test analysis. Values are presented as mean and error bars indicate standard errors (SE). To evaluate the hyaline cartilage forming potential, the ratio of COL2A1 to COL1A1 was expressed as $2^{-(Ct^{COL2A1}-Ct^{GAPDH})}/2^{(Ct^{COL1A1}-Ct^{GAPDH})}$ [25,26].

### 2.11. Transmission Electron Microscopy (TEM) on spheroids

Spheroids samples were collected at day 4, 7 and 14, washed with phosphate buffer 100 mM, pH 7.4, and fixed with glutaraldehyde 2.5 %

**Table 1**
Primers employed for Real-Time PCR tests.

| Primer | Sequence (5′ - 3′) |
|---|---|
| GAPDH_FW | TCAAGGCTGAGAACGGGAAG |
| GAPDH_REV | CGCCCCACTTGATTTTGGAG |
| COL1A1_FW | CCCTGGAAAGAATGGAGATGAT |
| COL1A1_REV | ACTGAAACCTCTGTGTCCCTTCA |
| COL2A1_FW | CCTGGCAAAGATGGTGAGACAG |
| COL2A1_REV | CCTGGTTTTCCACCTTCACCTG |
| SOX-9_FW | AGGAAGCTCGCGGACCAGTAC |
| SOX-9_REV | GGTGGTCCTTCTTGTGCTGCAC |
| COL10A1_FW | CAAGGCACCATCTCCAGGAA |
| COL10A1_REV | AAAGGGTATTTGTGGCAGCATATT |

(*w/v*) in phosphate buffer 100 mM, pH 7.4, for 2.5 h at 4 °C. The fixative was removed and fresh phosphate buffer was added to each sample. After short washing steps in phosphate buffer 100 mM, the samples were post fixed in osmium tetroxide ($OsO_4$) 1 % in cacodylate buffer 100 mM for 30 min at 4 °C and then embedded in epoxy resin after a graded acetone serial dehydration step (30 %, 50 %, 70 %, 90 %, 100 % *v*/v in $H_2O$). Ultrathin sections of 100 nm were stained by uranyl acetate solution and lead citrate, and then observed by transmission electron microscope CM10 Philips (FEI Company, Eindhoven, The Netherlands) at an accelerating voltage of 80 kV. Images were recorded by Megaview III digital camera (FEI Company, Eindhoven, The Netherlands).

### 2.12. Immunohistochemistry on spheroids (Type-2 collagen) and image analysis

Spheroids samples were collected at day 4 and 7 to evaluate the expression of type-2 collagen by immunohistochemical analyses. The spheroid samples were fixed with formaldehyde 4 % *V*/V (Sigma) in PBS for 30 min at room temperature, washed with PBS 1× and incubated with Triton-X100 0.2 % *v*/v for 15 min at room temperature and then with a blocking solution containing Bovine Serum Albumin (BSA) 4 % *w/v* and Normal Goat Serum (NGS) 5 % in PBS 1×, for 1 h at room temperature (RT). The blocking solution was then removed and spheroids were washed with PBS 1×. The collagen II monoclonal antibody was diluted in blocking buffer (1:200) and incubated with the spheroids at 4 °C over night. A washing step was performed with PBS 1× and incubated with the secondary antibody diluted in blocking buffer (1:200) for 2 h at room temperature. The samples were washed with PBS 1× and the cell nuclei were counterstained with DAPI. The samples were washed with PBS 1× and mounted on a microscope slide with Mowiol. Images were acquired using a Nikon C1si confocal microscope (Nikon, Tokyo, Japan), equipped with 488 nm (argon), 408 nm, and 561 nm (diode) lasers. Light was delivered to the sample with an 80/20 reflector. The system was operated with a pinhole size of one Airy disk. Electronic zoom was kept at minimum values for measurements to reduce potential bleaching. For the different fields collected we used a 40× Plan Apo objective at different *Z*-stacks at 318 μm × 318 μm. Images were captured under identical acquisition settings in order to allow comparison of fluorescent intensity. The staining quantification was performed and analyzed by the Fiji-ImageJ 1.53c tool ROI manager (NIH, Bethesda, USA). Images of four different spheroids were analyzed for each sample. The fluorescence intensity was expressed as CTCF/ selected Area where CTCF = Integrated Density – (Selected Area X Mean fluorescence of background readings).

### 2.13. ELISA assay for Type-2 collagen quantification in spheroids

Type-2 collagen was measured by quantifying C-terminal propeptides in spheroid medium at day 4 and 7 after cell seeding, using the Human CTXII ELISA Kit (FineTest) following the manufacturer's instructions. Optical density was measured using a FLUOStar Omega-BMG Labtech spectrophotometer. Data was normalized to the total protein content evaluated a by microBCA assay (ThermoFisher Scientific) in spheroid lysates according to manufacturer's instructions.

## 3. Results

### 3.1. Formation and morphological characterization of CTL-spheroids

Spheroids based on hMSCs and CTL were generated using a procedure previously described by the authors for the production of chondro-aggregates [17]. In brief, cells were seeded onto CTL-coated tissue culture wells, which were prepared by air-drying a polymer solution. In the present work, the spheroids produced on the CTL-coating are referred to as CTL-spheroids. The properties and features of CTL-spheroids were compared with those of spheroids obtained by seeding the cells onto a non-adherent surface consisting of an agar gel, and referred hereafter to as MF-spheroids (Matrix-Free spheroids) (Fig. 1a-b).

After cell seeding in chondrogenic differentiation medium, the progression of CTL- (Fig. 1c-h) and MF-spheroid formation (Fig. 1i-p) was monitored from day 1 to day 21 by optical microscopy. Under both conditions, the cells do not adhere and they begin to self-assemble into small aggregates already from day 1. As the culture time progresses, these aggregates organize themselves into spherical structures with increasingly larger diameters and higher cell density. Although the general behavior of the spheroids over time is the same, clear differences can be observed between the two systems. Indeed, the MF-spheroids already show a larger size with respect to CTL-spheroids on the first days of culture, although a considerable size heterogeneity occurs in both cases. This difference becomes even more evident in the following period, in which the formation of fewer structures with larger diameters occurs, mainly due to a process of coalescence of already formed aggregates. In the case of MF-spheroids, the aggregates display a diameter in the range of 97 ± 43 μm and 194 ± 128 μm at day 1 and day 4, respectively. In the case of CTL-spheroids the dimensions are in the range of 50 ± 16 μm and 114 ± 59 μm in the same culture period. From day 7 onwards, the presence of a single spheroid can be observed in the agar-coated wells (diameter in the range 300–500 μm) while in the CTL-coated wells both single and only partially fused spheroids are still clearly visible at day 14. Only from this point on, the dimensions of the two types of spheroids become comparable. A more detailed analysis of the morphology of the spheroids is provided by SEM images (Fig. 2). In both culture conditions, already at day 4, defined cell boundaries are no longer recognizable in the aggregates, but the structures already appear quite compact and rather smooth. At day 4, the surface of the CTL-spheroids appears somewhat more irregular, with higher magnification also revealing individual cells in an amorphous matrix; this appears also on spheroids at day 11 (see inset in Fig. 2.a1 and c1). Over time, the structures become larger, very compact and dense, and the phenomenon of coalescence becomes evident.

Cell viability in the spheroids was evaluated by the Alamar Blue assay (Fig. 3a). The results show that, although a progressive decrease in cell viability occurred over 14-days culture for both spheroid types, in CTL-spheroids an increase of fluorescence signal occurs from day 1 to day 4, indicating some degree of cell replication.

A qualitative assessment of cell viability was also performed using a live/dead assay, which is based on the differential permeability of live and dead cells to a pair of fluorescent dyes (calcein-AM staining for living cells and propidium iodide for dead cells). The test shows that the cells composing the spheroids are viable in both samples at day 1, when the size of the spheroids is sufficiently small to allow oxygen and nutrient diffusion through the structures (Fig. 3b and c). As the diameter of the spheroids increases, a necrotic core surrounded by a crown of viable cells form (Fig. 3d-i). The formation of the necrotic core in spheroids has been reported for different spheroid types [27] and it can be ascribed to their compact structure, which prevents the diffusion of oxygen and nutrients [28,29]. The occurrence of this phenomenon is particularly evident from day 4 only in MF-spheroids for which, due to the large dimensions of spheroids, the extent of cell death progresses gradually during the 14-day spheroid culture. Conversely, in CTL-spheroids the presence of the polymer retards the process of cell aggregation, which results in the formation of spheroids with smaller dimensions and thus to an increase of the overall cell viability.

The ability of CTL to promote the aggregation of chondrocytes and to act as a temporary and bioresorbable extracellular matrix through the interaction with sugar-binding membrane structures have already been reported by some authors of this paper [17]. On this basis, the localization of CTL in the MSC-spheroids was assessed by seeding the cells onto a coating of CTL labelled with the FITC fluorochrome (Fig. 4).

The images show that the fluorescent CTL is mainly located in the inner part of the spheroids (Fig. 4a-h). In analogy to what was observed

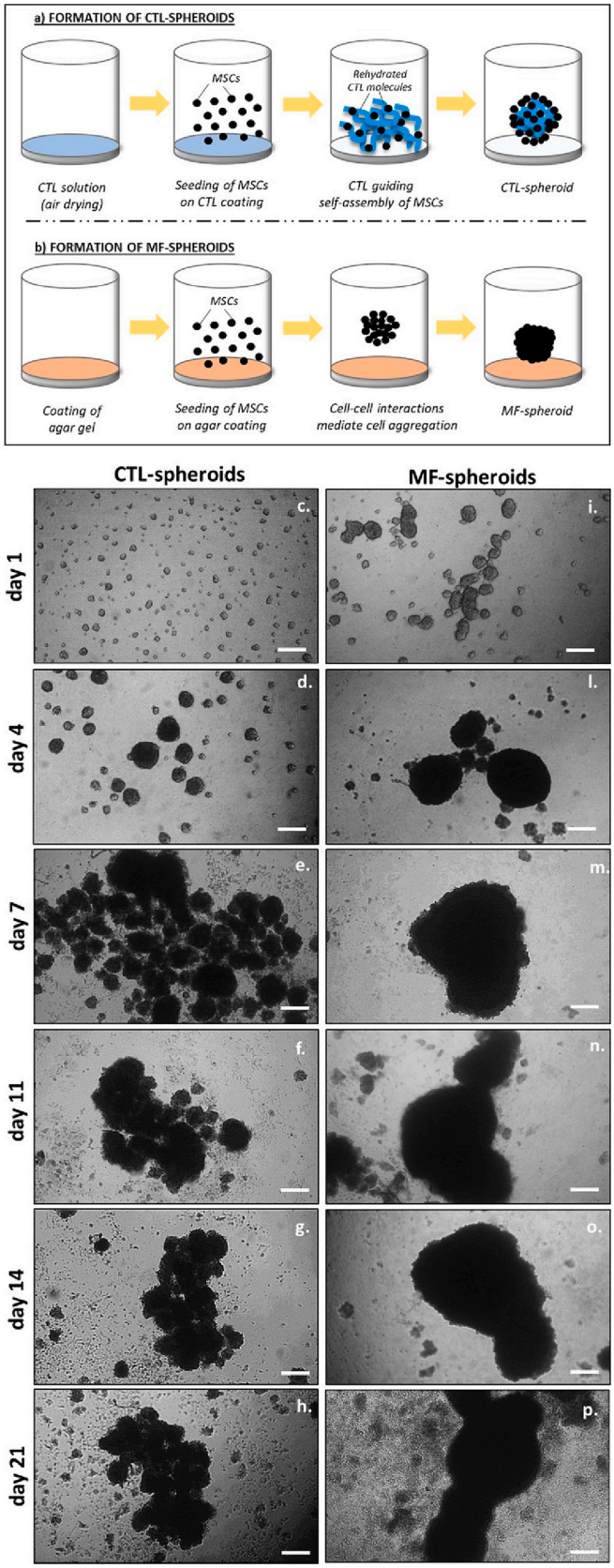


*(caption on next column)*

**Fig. 1. Schematic illustration of the CTL- (a) and MF-spheroids (b) formation, and optical images of CTL-spheroids (c-h) and MF-spheroids (i-p) (scale bar: 200 μm).** hMSCs are seeded on an air-dried CTL coating. During the rehydration process, the polymer chains are dissolved in the culture medium and form an extracellular matrix in hybrid, spherical cell-CTL structures through cell-polymer interactions (a). In MF-spheroids, hMSCs are seeded on an agar gel; spheroid formation occurs through the establishment of cell-cell interactions (b1). Optical images of CTL- (c, d, e, f, g, h) and MF-spheroids (i, l, m, n, o, p) describing the progression of spheroid formation over time (day 1, 4, 7, 11, 14 and 21, respectively).

in aggregates based on chondrocytes, it can be assumed that the cells in these structures can bind to CTL and simultaneously interact with themselves, leading to the formation of hybrid polymer-cell structures in which the polymer is embedded. No variation in CTL localization within spheroids is observed over time.

### *3.2. Chondrogenic differentiation capabilities and expression of stemness markers in CTL-spheroids*

In order to evaluate the chondrogenic gene expression in spheroids, quantitative Real Time PCR (qPCR) analyses were carried out to track the relative variations in COL2A1, SOX-9, COL1A1, and COL10A1 expression in differentiation medium. The results reflect the expression snapshots of the aforementioned genes at days 0, 4, 7, 14 and 21, and the COL2A1:COL1A1 mRNA ratio in both CTL-spheroids and MF-spheroids (Fig. 5a-c).

In MF-spheroids, COL2A1 expression did not increase significantly until day 21, when only a ~2-fold increase can be observed (Fig. 5a); this time frame is consistent with data reported in the literature on the kinetics of stem cell differentiation in 3D systems [6,30,31]. Surprisingly, the chondrogenic differentiation marker COL2A1 was remarkably upregulated in CTL-spheroids. The amount of COL2A1 mRNA increased significantly at early time points, and at day 4 the expression was about 700-fold higher than at day 0 (Fig. 5a). This time point corresponds to the highest spheroid viability and to the lowest spheroid dimensions. After day 4, the level of COL2A1 mRNA decreased. However, it is interesting to note that the expression level of COL2A1 at day 7 was still 40 times higher than at day 0, and it continued to increase at day 21 (day 7: ~40×; day 14: ~30×; day 21: ~86× than day 0, respectively).

SOX-9 is a pivotal transcription factor in developing of cartilage and it is active throughout chondrocyte differentiation. This transcriptional activator directly targets genes encoding key cartilage-specific extracellular matrix components such as collagen types 2, 9, and 11, aggrecan, link proteins and their regulators [32]. The expression profile of SOX-9 differed between the two culture systems (CTL- and MF-spheroids). In the CTL system, there was an initial increase in its mRNA levels as early as day 4, reaching its peak at day 7, followed by a decline in its expression at day 14, and an increase again at day 21. Conversely, in MF-spheroids the expression of SOX-9 seemed to decrease throughout the culture period until day 14 and showed an increase only at day 21 (Fig. 5b).

The expression of COL1A1 and COL10A1 was also considered, since these genes are markers of endochondral bone formation and hypertrophy, respectively, and they negatively correlate with the chondrogenic differentiation of stem cells. The expression of COL10A1 did not change significantly at all time points compared to day 0 in both spheroid types (data not shown). As to the second marker, the ratio between COL2A1 and COL1A1 mRNA levels is commonly used as an indicator of the mature chondrocyte phenotype in gene expression analysis [33,34]. The COL2A1:COL1A1 mRNA ratio showed a consistent upward trend in the MF-spheroids, but never exceeded the value of 2.0 by day 21 (Fig. 5c). In contrast, chondrogenic differentiation in CTL-spheroids showed a strong increase in COL2A1:COL1A1 mRNA ratio over time, reaching a value of ~160-fold at day 21 of culture. This substantial increase suggested an enhancement in the chondrocyte-

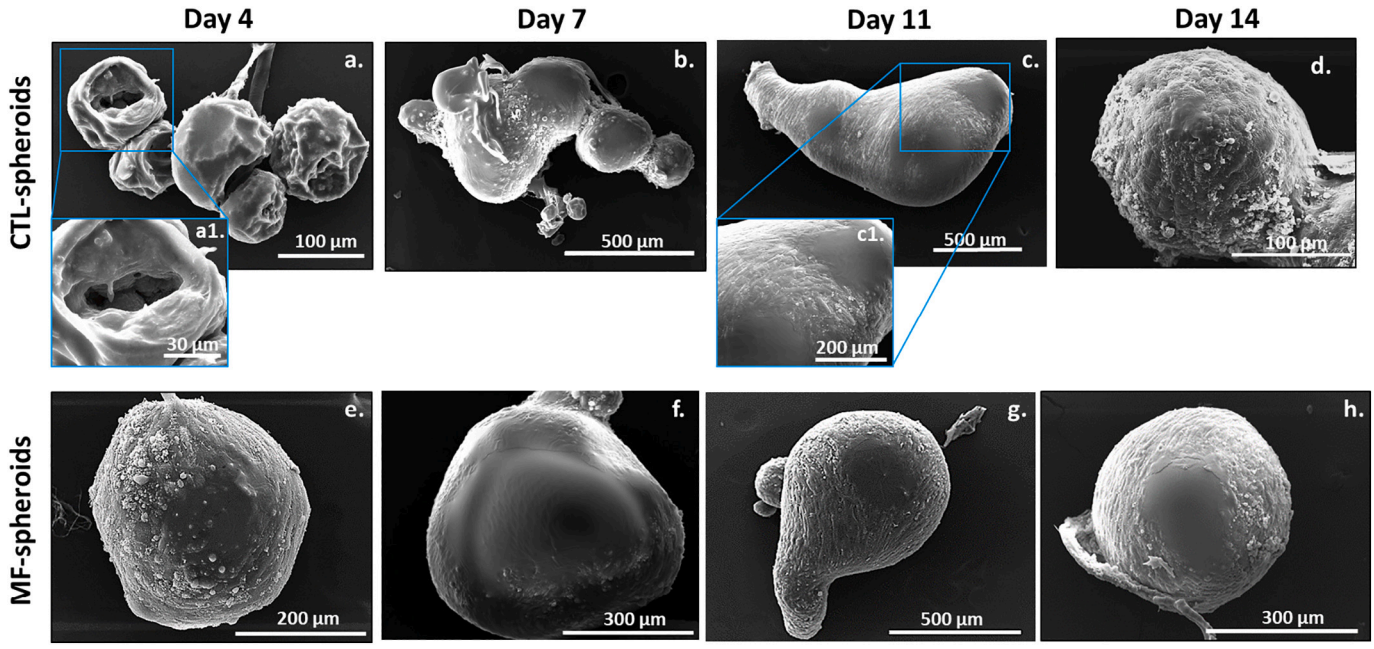


**Fig. 2. SEM images of CTL-spheroids (a, b, c, d) and MF-spheroids (e, f, g, h) at day 4, 7, 11 and 14 of culture.** Insets: details of individual cells embedded in an amorphous matrix in CTL-spheroids (a1); external matrix of CTL-spheroids (c1). (Scale bar a1: 30 µm; a. d.: 100 µm; e, c1: 200 µm; f. h.: 300 µm; b. c. g.: 500 µm).

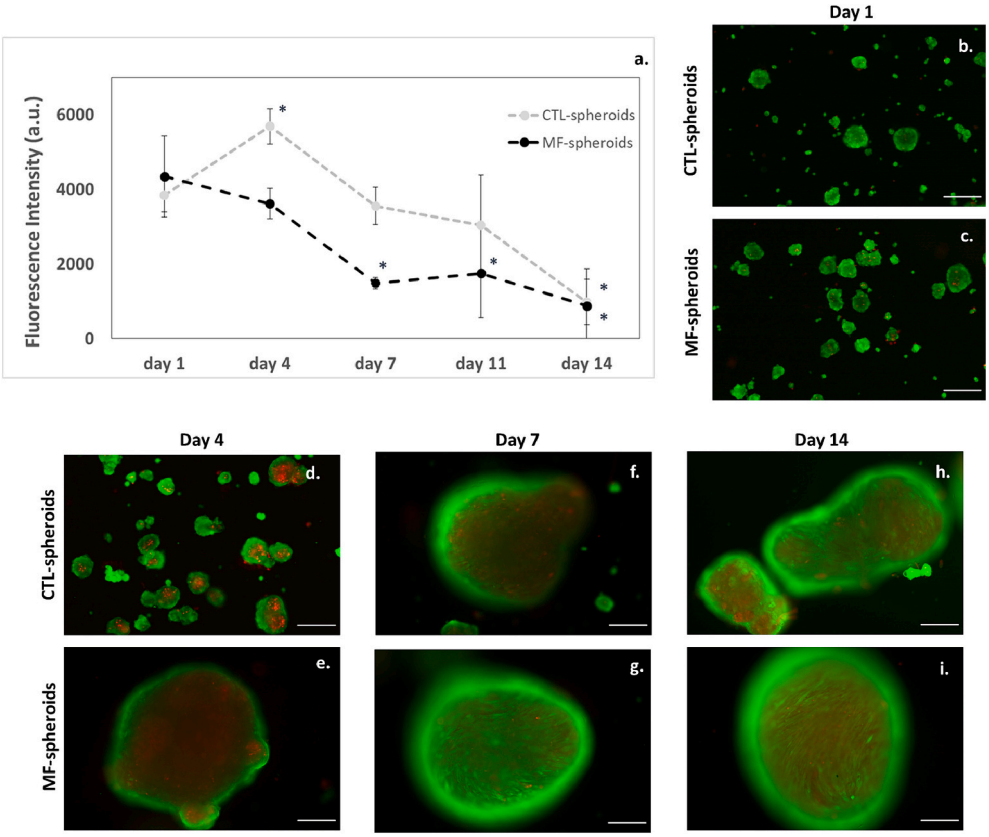


**Fig. 3. Alamar blue assay (a) and Live/dead images of CTL-spheroids (b, d, f, h) and MF-spheroids (c, e, g, and i) at day 1, 4, 7 and 14 (scale bar: 200 µm).** Living cells are in green, while dead cells appear in red. For Alamar blue assay (a), data are reported as mean ± standard deviation ($n = 5$). Statistics: unpaired Student's *t*-test (*: *p*-value $< 0.05$). (For interpretation of the references to colour in this figure legend, the reader is referred to the web version of this article.)

specific phenotype compared to MF-spheroids.

Additionally, considering that the nature and composition of the extracellular niche is of pivotal importance not only for the differentiation capacity but also for the maintenance of the pluripotent and self-renewing state of stem cells, the expression of the self-renewal genes NANOG and OCT-4 in CTL- and MF-spheroids was also

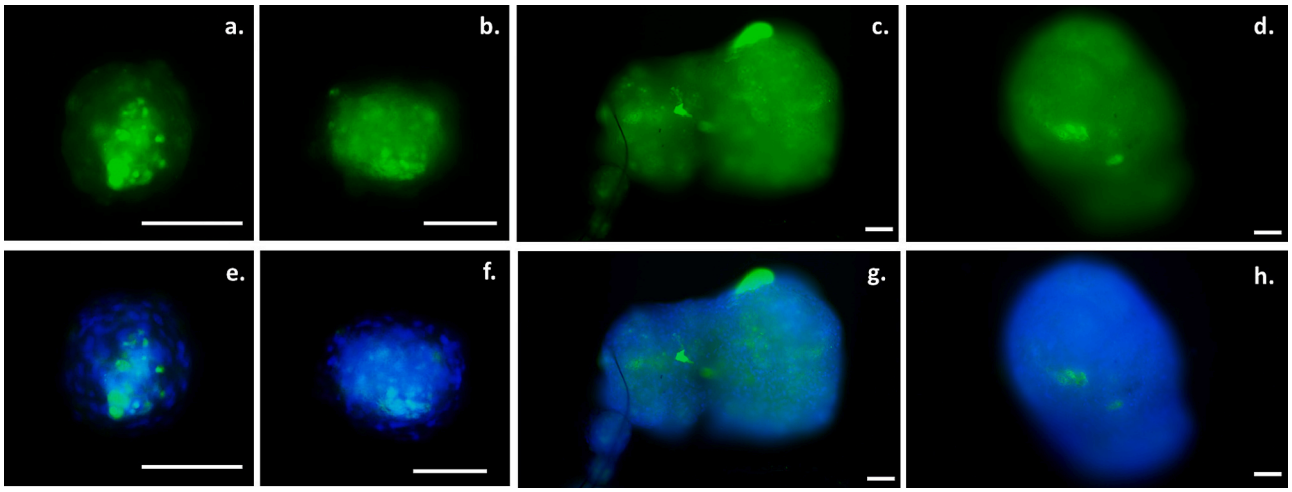


**Fig. 4. Localization of CTL in CTL-spheroids at day 1 (a, e), 4 (b, f), 7 (c, g) and 14 (d, h).** Green fluorescence corresponds to FITC-labelled CTL; blue fluorescence corresponds to cell nuclei stained with Hoechst (scale bar: 100 μm). (For interpretation of the references to colour in this figure legend, the reader is referred to the web version of this article.)

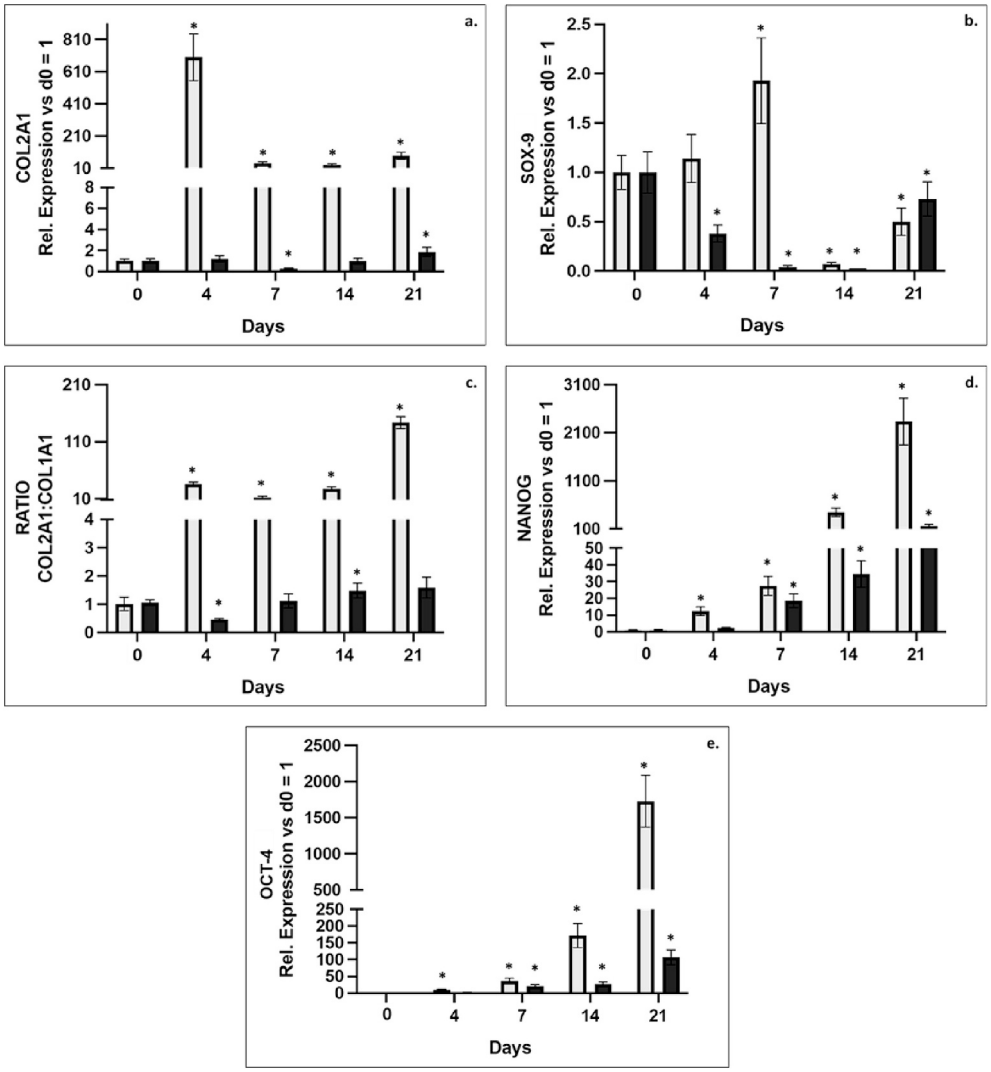


**Fig. 5. Kinetic study of gene expression in CTL-spheroids and MF-spheroids (a-e).** Expression of COL2A1 (a), SOX-9 (b), ratio COL2A1:COL1A1 (c), NANOG (d), OCT-4 (e) in CTL-spheroids (grey bars) and MF-spheroids (black bars). The ratios of COL2A1:COL1A1 at each time point were calculated as described in the Materials and Methods section. The data were normalized to the housekeeping gene GAPDH, and the relative expression of each gene was calibrated to that of day 0 cells (set as 1). Data are presented as mean ± SE (*: $p$-value < 0.05).

investigated after 4, 7, 14 and 21 days in differentiation medium (Fig. 5d-e).

These findings revealed a comparable expression pattern over time in both culture systems, although with variable relative expression levels at each time point. Despite being conducted under differentiation conditions, the genes in both cases exhibited a time-dependent increase as early as day 4, but CTL-spheroids demonstrated a greater increase compared to MF-spheroids. For instance, in CTL-spheroids, the relative expression of NANOG escalated from approximately 12-fold at day 4 to around 2300-fold at day 21, whereas in MF-spheroids, the upregulation ranged from approximately 2-fold to about 150-fold, respectively. Similar trends were observed for OCT-4 expression levels.

Type-2 collagen expression was examined by immunohistochemistry at day 4 and day 7 of spheroid culture, as an upregulation of the COL2A1 gene in CTL-spheroids occurred within the first week of culture (Fig. 6a-i). Image analysis was performed using ImageJ software tools to quantitatively measure the fluorescence intensity. The results show that type-2 collagen is present at low levels in both samples on day 4 of culture, although it appears significantly more highly expressed in the CTL-spheroids. On day 7, however, the two samples show the greatest differences. While the level of protein expression does not change in MF-spheroids, the fluorescence signal more than doubles in CTL-spheroids. The data are also confirmed by the quantification of type 2-collagen telopeptides in the growth medium of CTL- and MF-spheroids on days 4 and 7 after seeding (Fig. 6l.)

Histological evaluation was done by H/E and Masson's Trichrome stainings in both CTL-spheroids and MF-spheroids (Fig. 7a-n). H/E staining confirmed the dimensional analysis reported in Section 3.1 "*Formation and morphological characterization of CTL-spheroids*", as CTL-spheroids have smaller dimensions and a less dense and compact structure than MF-spheroids (Fig. 7a-f).

In terms of structural organization, cells in CTL-spheroids were preferentially localized at the edge of the structure (black arrows) rather than in the spheroid core, where an amorphous matrix is deposited (blue arrows). The latter can be associated with CTL because of its ability to bind the dye [17]. The hypothesis is consistent with the images with FITC-labelled CTL, showing that the polymer is predominantly located inside the aggregates (Fig. 4). Interestingly, conversely to MF-spheroids, in CTL-spheroids cell arrangement within the structure seems to reproduce chondroblasts/osteoblasts within chondrogenic osteogenic lacunae [35]. This resemblance became particularly evident after 4 days of culture (Fig. 7a).

Masson's Trichrome staining, which highlights collagen fibers in blue (black arrows), showed that there was an early deposition of collagen-based extracellular matrix in CTL-spheroids starting from day 4 of culture (Fig. 7g). This deposition remained consistent throughout all experimental time points, with the blue staining becoming even more intense after 7 and 14 days of culture (Fig. 7h-i). Conversely, in MF-spheroids at day 4, 7 and 14, a clear blue staining was observed only at day 7 of culture and appeared weaker at day 14, when a weak blue signal appeared within a compact cellularized matrix (Fig. 7i -n).

### 3.3. TEM ultrastructural analysis of CTL-spheroids

Transmission Electron Microscopy (TEM) analyses were performed in order to characterize the ultrastructural morphological organization of spheroids, in terms of ECM deposition, interaction between CTL and cells, and the cellular modifications correlated to CTL. Fig. 8 shows CTL-spheroids cultured for 4, 7 and 14 days.

After 4 days of culture, a well-organized and compact structure is observed. At low magnification, nuclei and nucleoli are easily observed, while cytoplasmic organelles and cell membrane are indistinguishable from the other components of the ECM (Fig. 8a). The rough endoplasmic reticulum (RER) is widely developed suggesting an intense protein synthesis (Fig. 8.a1). Several lysosome and vesicles are observed inside the cytoplasm, which are correlated with the interaction between cells

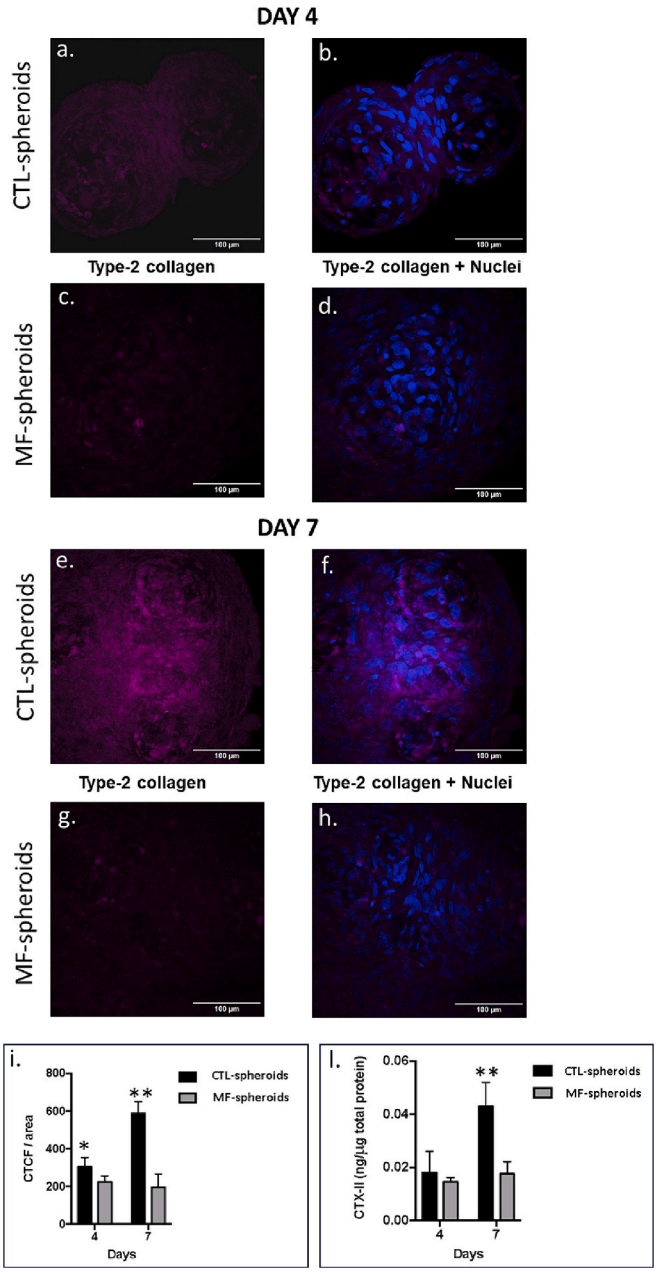


**Fig. 6. Immunohistochemical images of CTL- (a, b, e, f) and MF-spheroids (c, d, g, h) showing type-2 collagen stained red, while the nuclei are stained blue (DAPI) (Scale bar 100 µm). (i) Quantitative analysis of fluorescence microscopy images of CTL- and MF-spheroids.** Data are presented as mean ± SE of the CTCF/selected area values of the analyzed images according to the formula described in Materials and Methods. (**l) Quantification by ELISA of type-2 collagen telopeptides (CTX-II) in CTL- and in MF-spheroids medium on days 4 and 7 after cell seeding**. Data representative of the experiment run in triplicate. Values are expressed as mean ± SD and are normalized to total protein content in spheroid lysate. Statistically significant differences between CTL- and MF-spheroids values were analyzed using Student's *t*-test. Symbols indicate statistical significance (**: $p$-value $< 0.01$; *: p-value $< 0.05$. For quantitative analysis of fluorescence microscopy images $n=4$; for ELISA assay $n=3$). (For interpretation of the references to colour in this figure legend, the reader is referred to the web version of this article.)

and the sugar-based components of CTL. In the ECM, fibrillary structures are detected (Fig. 8b). At higher magnification a banding organization resembling the collagen type-2 proteins is easily detected (Fig. 8.b1).

After 7 days of cell culture, cells showed a well preserved

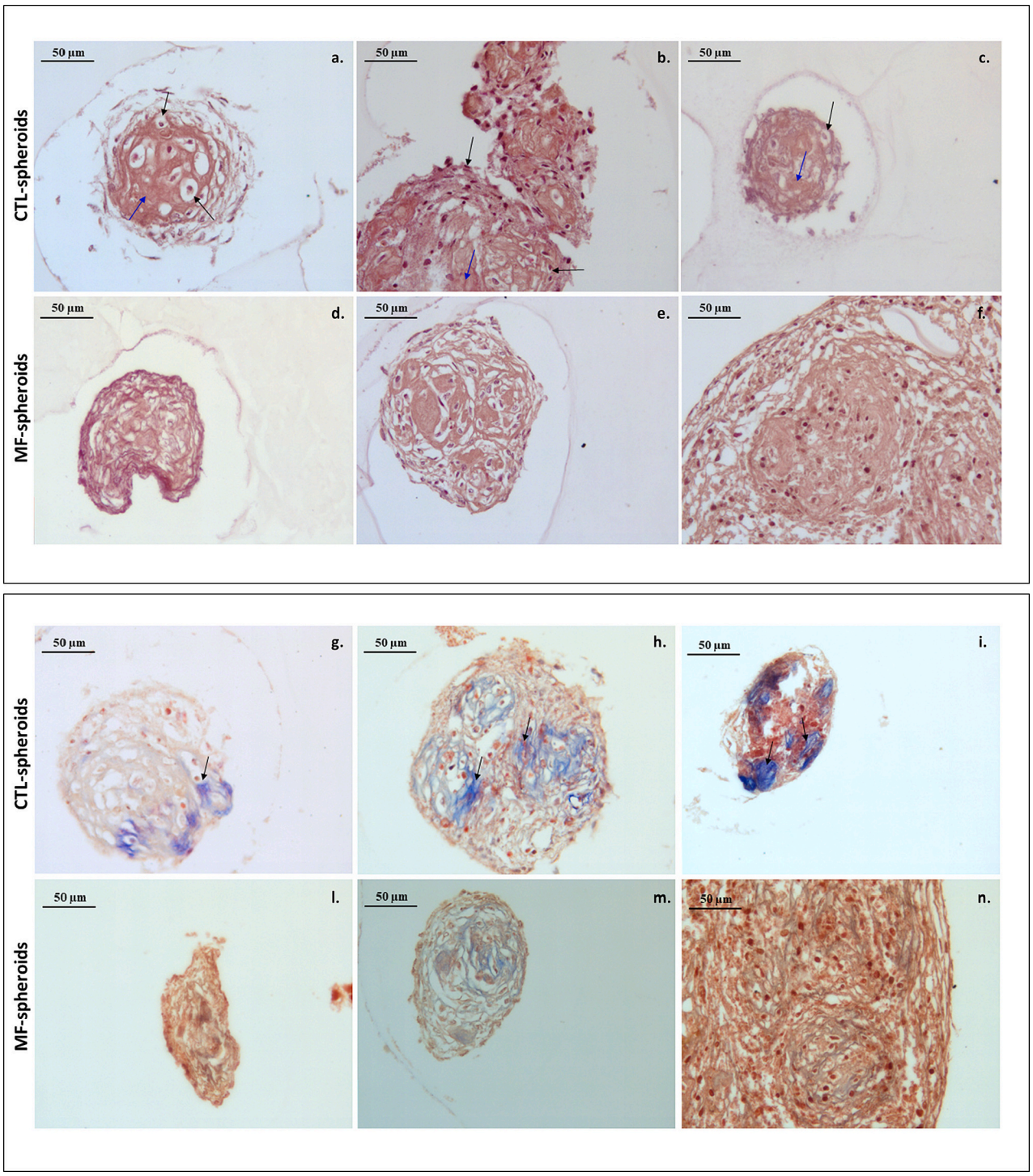


**Fig. 7. H/E staining on CTL- (a, b, c) and MF-spheroids (d, e, f) at day 4, 7 and 14 (scale bar: 50 µm), and Masson's Trichrome on CTL- (g, h, i) and MF-spheroids (l, m, n) at 4, 7 and 14 days of culture (scale bar: 50 µm).** Blue staining identifies collagen. (For interpretation of the references to colour in this figure legend, the reader is referred to the web version of this article.)

morphology (Fig. 8c) and an increased deposition of collagen fibers is detected in the ECM (Fig. 8d). Lysosomes are still observed inside the cytoplasm (Fig. 8.c1), while the RER almost filled the cytoplasmic area. Collagen fibers parallel, perpendicular oriented and with a banding structure are detected in the ECM (Fig. 8d and .d1).

After 14 days of CTL culture, the spheroids showed a preserved morphology only in cells localized on the external surface while degraded ECM and several necrotic cells are observed in the inner area (Fig. 8e). Empty vesicles are visible and a deteriorated ECM is shown (Fig. 8f). Collagen fibers are still detected but no clear banding structure is still observed, suggesting protein degradation correlated with cell death (Fig. 8f and .f1).

In MF-spheroids at day 4, the cells show a preserved cellular ultrastructural morphology (Fig. 9a).

Large empty spaces between cells are clearly observed at low magnification (Fig. 9a), suggesting a low production of ECM components. The single cells are easily detected, including nuclei and cell membrane (Fig. 9a). At higher magnification, the cells show a well-

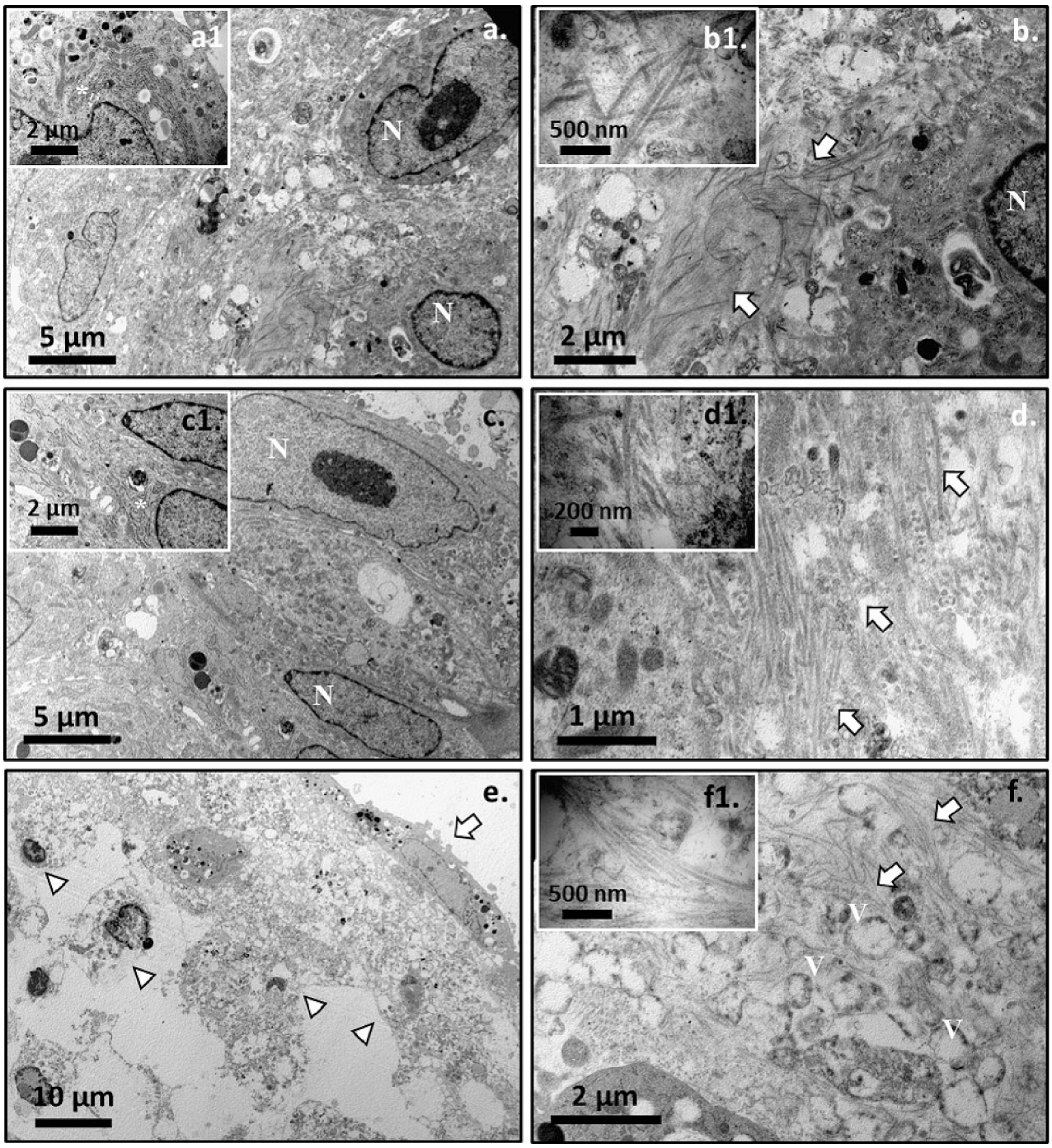


**Fig. 8. Representative images of TEM ultrastructural morphological analysis of CTL spheroids.** Low magnification of the internal organization of CTL-spheroids after 4 days of cell culture (a). Nuclei are easily detected (N) while the cytoplasmic components are indistinguishable from the other components of the ECM. Cellular organelles such as mitochondria and RER (a1) are observed (bar: 5 µm; bar inset: 2 µm); detail of the ECM in which fibrillar structures (arrows) are observed (b). A banding organization in the fibrillar components is easily detected (b1) (bar: 2 µm; bar inset: 500 nm); CTL spheroids after 7 days of cell culture (c). Cells show a well preserved morphology and are tightly connected each other. Nuclei (N) and RER (c1) are easily detectable (bar: 5 µm; bar inset: 2 µm); ECM detail showing filaments structures parallel oriented (arrows) (d). A banding organization is still detectable in the filamentous component of ECM (d1) (bar: 1 µm; bar inset: 200 nm); CTL spheroids after 14 days of cell culture (e). Several necrotic cells (arrow heads) are observed in the internal structure of the spheroids, while elongated and well preserved cells are detected on the external surface (arrows) (bar: 10 µm). Fibrillar components (arrows) and several vesicles (V) in the ECM are detected (f). No banding organization in the fibrillar structures is detected (f1) (bar: 2 µm; bar inset: 500 nm).

developed RER (Fig. 9.a1). A detail of ECM show a less compact organization compared to CTL samples, (Fig. 9b). In these spheroids a few fibrillar component is detected and a clear banding structure is missing (Fig. 9b and .b1), suggesting the inability of the cells to complete the process of collagen maturation. After 7 days of culture, empty spaces between cells are still observed in MF-spheroids (Fig. 9c). The ultrastructural cellular morphology shows a developed RER, filling half of the cytoplasm (Fig. 9.c1). In these structures, the ECM is characterized by empty spaces and several fibrillar components, parallel oriented, in which no banding structure is detected (Fig. 9d and .d1). After 14 days of culture, the cells composing the spheroids do not show any sign of cellular damage and/or death (Fig. 9e). They show a preserved

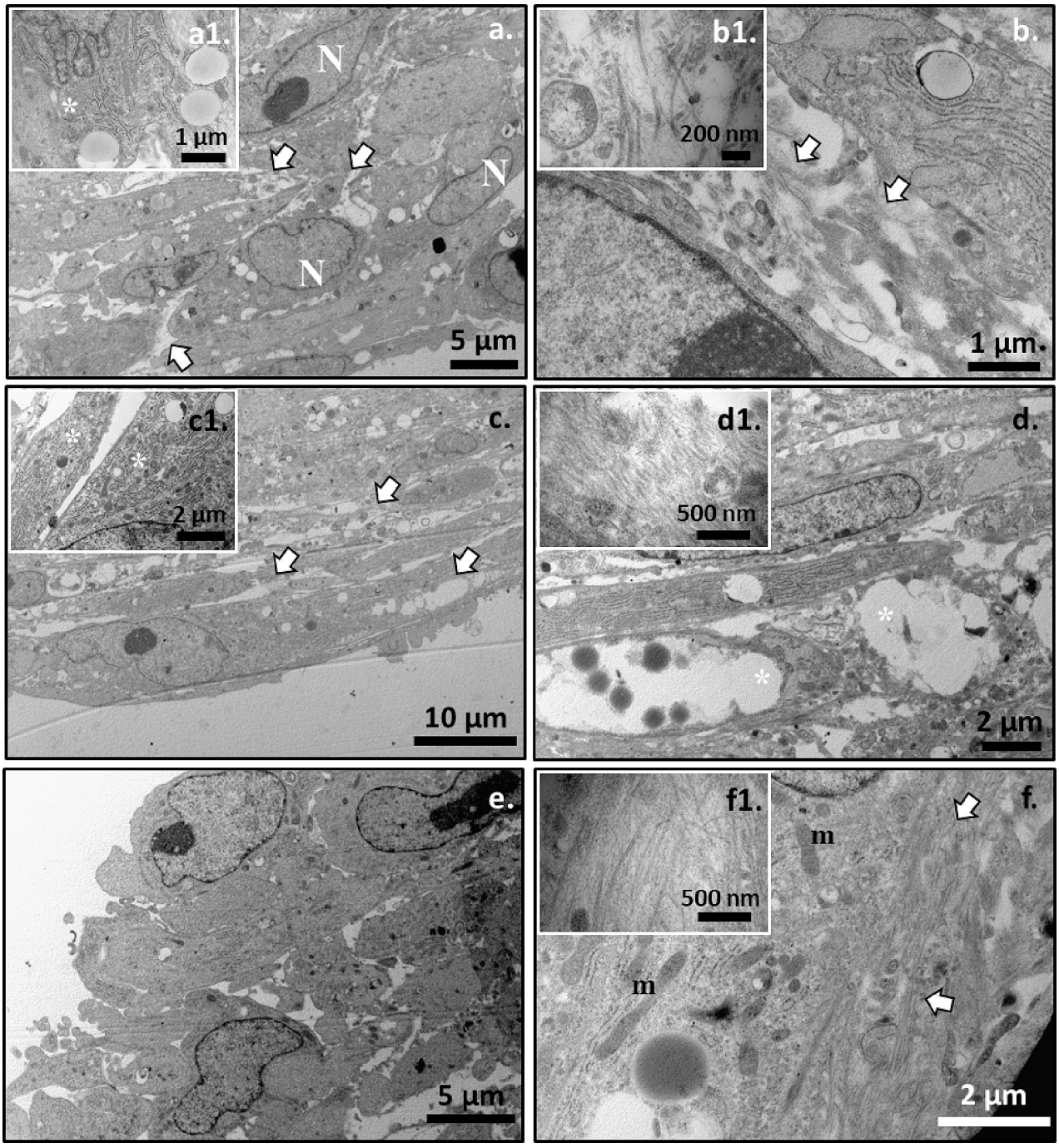


**Fig. 9. Representative images of TEM ultrastructural morphological analysis of MF-spheroids.** Cells after 4 days of culture showed a well preserved morphology (a). Nuclei (N) are easily observed. Several areas of empty spaces are detected between cells (arrows). RER (a1) and Golgi complex are observed in the cells, suggesting a high metabolic activity (bar: 5 µm; bar inset: 1 µm); In the space between cells, a few fibrillar components of the ECM (arrows) are detected (b). No banding organization is observed in the ECM filaments (b1) (bar: 1 µm; bar inset: 200 nm); Cells after 7 days of agar culture still showed space (arrows) between each other (c). Cell morphology is preserved in the outer surface and inner structure of the agar spheroid. Well developed RER (*) is observed in the cytoplasm (c1) (bar: 10 µm; bar inset: 2 µm); Detail of the ECM showing a few fibrillar components and large empty areas (*) between cells (d). Fibrillar components of the ECM are parallel oriented but do not show any banding organization (d1) (bar: 2 µm; bar inset: 500 nm); Cells after 14 days of agar culture (e). Cells still showed a well preserved morphology although empty spaces between them are observed. No sign of cell death is detected (bar: 5 µm); Cellular organelles such as mitochondria (m) are observed, while a few fibrillar component are observed in the ECM (arrows) (f). At higher magnification no banding organization is observed in the fibrillar components of ECM (f1) (bar: 2 µm; bar inset: 500 nm).

morphology, in which cell nuclei, cellular organelles, RER and mitochondriaare easily detected (Fig. 9e and f). Empty spaces between cells were observed, suggesting a low production of ECM components even after 14 days of culture. At higher magnification, a few fibrillar structures were detected in the ECM (Fig. 9f and .f1) but no sign of banding organization was observed (Figure 9.f1).

## 4. Discussion

MSCs represent one of the main cell sources for applications in tissue

regeneration. The regenerative potential of MSCs led researches to investigate additional features of these cells, such as the presence of extracellular vescicles (ECVs) secreted by cells to treat bone and cartilage-related diseases [36–38] and their ability to form spheroids.

MSCs-spheroids have shown potential for the treatment of various diseases and injuries affecting cartilage tissue, due to their ability to replicate the three-dimensional microenvironment of natural tissues. However, cartilage regeneration is a time-consuming process, as chondrogenic differentiation requires 21 days of in vitro culture prior to implantation, a time-frame that can result in a dramatic reduction in spheroid viability. The achievement of successful cartilage regeneration outcomes may rely on innovative strategies aimed at accelerating the process of chondrogenic differentiation, while maintaining viable cell structures. In the present paper, this aim was pursued by the use of a naturally derived polysaccharide, namely CTL, for the preparation of polymer-cell spheroids.

While CTL and its biochemical features have been previously documented in the context of cartilage tissue engineering, these results shed light on three important innovative contributions: (i) the acceleration of chondrogenic differentiation, (ii) the feasibility of early implantation of differentiated spheroid structures and (iii) the form in which CTL can employed. Specifically, CTL-spheroids show accelerated chondrogenic differentiation which is achieved within approximately one week of cell culture, as opposed to conventional approaches that require approximately 21 days. This accelerated time frame has potential implications for shortening the duration of the surgical procedure, minimizing costs, and improving patient outcomes by implanting spheroids composed of viable and differentiated cells.

Spheroids were prepared by a simple method based on seeding MSCs onto an air-dried coating of CTL (Fig. 1a). In this approach, the polymer CTL plays a dual role: (*i*) the air-dried coating inhibits cell adhesion to the substrate immediately upon cell seeding and, (*ii*) during rehydration, the CTL molecules are included in the spheroid structure, where they may serve as a structuring matrix that binds the cells through the interaction with membrane proteins [17]. As suggested by the presence of the polymer inside the structures (Fig. 4), in CTL-spheroids a combination of cell-cell and cell-CTL interactions occurs simultaneously, which prevents the fusion of the aggregates into larger structures. In this case, it is reasonable to assume that, upon cell seeding, the polymer creates a steric hindrance among cells, preventing them from aggregating into large structures.

The process of spheroid formation in the presence of CTL differs slightly from that observed in the control (MF-spheroids), where cell aggregation occurs essentially by preventing cell adhesion through a layer made of an agar gel (Fig. 1b). These two different mechanisms of spheroid formation account for the different size that the spheroids reach at each time point. Indeed, in MF-spheroids the prevalence of cell-cell interactions leads to the formation of few, large, dense spheroids from day 4 onward. In this case, the coalescence of the existing aggregates progresses rapidly and an almost single spheroid can be observed starting from day 7 (Fig. 1c-p).

This might explain why CTL- and MF-spheroids do not reach comparable dimensions until the fourteenth day of culture. The smaller size and lower cell density could also be the reason for the higher viability of the cells in CTL-spheroids, especially in the first days of culture (Fig. 3a).

Indeed, the results in Fig. 3a show an increase of cell viability for CTL-spheroids from day 1 to day 4, followed by a progressive decrease of the signal over time. In the case of MF-spheroids, the viability of cells is already reduced at day 4, which can be ascribed to the formation of larger and more compact spheroids due to a phenomenon of cell aggregation. In MF-spheroids, it can be appreciated the formation of a necrotic core that often correlates with the diameter of the spheroids and with their compact structure, which hinders the diffusion of gases and nutrients, leading to hypoxia and necrosis of cells located in the central region [27,29].

In this view, the culturing of cells on an air-dried CTL coating seems to be a promising strategy to improve the viability of spheroids, by slowing down the formation of larger aggregates.

Regarding the need to achieve a faster differentiation, it has been reported that the incorporation of an external ECM at the early stages of spheroid formation results in an increased survival and osteogenic differentiation [39]. This suggests that the niche established by the ECM and in which the cells are embedded may be crucial for the functions of MSCs already at the early stages of spheroids formation. In this perspective, MF-spheroids display some limitations for applications in TE, since the cells secrete their own ECM only at later stages. Thus, the early incorporation of a biological matrix may represent an efficient strategy to enhance the overall effectiveness of spheroid-based approaches. Different strategies to increase cell-ECM interactions in spheroids have been tried in order to improve the stem cell functions and differentiation abilities of MSC spheroids. For example, hMSC spheroids cultured on a polymer film surface of poly(2,4,6,8-tetravinyl-2,4,6,8-tetramethyl cyclotetrasiloxane) display an improvement in self-renewal abilities, pro-angiogenic potency, and multilineage differentiation capabilities [40]. Similarly, fibronectin-adsorbed graphene flakes incorporated into MSC spheroids showed an enhancement of cell-ECM interactions and, subsequently, of the expression of paracrine factors for myocardial repair [41]. However, these methods often require either the use of synthetic matrices or complicated procedures that can limit their applicability at the clinical level.

As to the role of CTL in accelerating chondrogenic differentiation, it can be speculated that the early incorporation of CTL within spheroids creates a niche in which the interplay between cells and this natural polysaccharide matrix is improved, thus favoring the onset of cellular responses that also occur in vivo. In this perspective, an important aspect to highlight is the examination of gene and protein expression levels related to chondrocyte differentiation, particularly COL2A1. In CTL-spheroids, the expression of the gene encoding type-2 collagen exhibits a significant 700-fold increase as early as day 4 of culture (Fig. 5a). This upregulation occurs much earlier compared to the control MF-spheroids (which reach their peak at day 21 with a 2-fold increase) and differs from what has been reported in the existing literature regarding the 3D culture of mesenchymal cells [6]. The peak of collagen expression at day 4 corresponds to the period of maximum cell viability and an average spheroid size of $<200$ μm, which is still small enough to ensure oxygen and nutrient transport to the interior of MSC spheroids [42].

Another element indicating a progressive commitment towards a mature chondrocyte phenotype is the COL2A1/COL1A1 mRNA ratio, which is already around the value of 50 at day 4, while no increase is observed on MF-spheroids in the same time-frame (Fig. 5c). These findings are also corroborated by optical and electron microscopic investigations, which highlight the presence of large and intense areas of mature collagen even at a very early stage of culture compared to MF-spheroids (Figs. 6–9). The expression trend of the SOX-9 gene, a key marker for the multistage chondrogenesis pathway, clearly suggests the initiation of the differentiation process as early as day 4 (Fig. 5b). This early differentiation was not observed in the MF-spheroids. These data are confirmed by analyzing type-2 collagen in the CTL and MF-spheroids by histological evaluation, by quantitative immunohistochemistry and by ELISA. Thus, the incorporation of CTL into spheroids foster chondrogenic differentiation. The mechanism underlying this biological effect could be dual in nature. On the one hand, the smaller size of spheroids associated with a looser structure may facilitate enhanced diffusion of nutrients and differentiation factors, even reaching the innermost cells of the core more easily and rapidly. However, the presence of physical, mechanical and biological cues creates a specific microenvironment through the mutual interaction of MSCs with the surrounding matrix. This microenvironment has the potential to influence stem cells and impact cell fate determination.

The interaction between CTL and the cells facilitates the close proximity and adhesion of cells to one another. Therefore, we are

tempted to speculate that CTL might able to contribute to the creation of a 3D structure by acting as a temporary niche, as previously observed for chondro-aggregates [17], and by interacting with cell-cell and cell-ECM adhesion molecules, as reported for chitosan [43–45]. Studies should be carried out to analyze in detail the mechanism of cell-CTL interaction. In this context, the involvement of cell receptors that are activated by this interaction and that may be involved in chondrogenic differentiation should be analyzed.

Surprisingly, the expression of COL2A1 (as well as of SOX-9), drops drastically at day 7, followed by a new growth trend with a peak at day 21 (~160 x). The low expression levels of COL1A1 and COL10A1 exclude that the downregulation of COL2A1 is due to a process of cellular dedifferentiation or cell hypertrophy. The reason for this probably lies in the phenomenon of cell necrosis, which is responsible for the drastic reduction in the viability of the cells between day 7 and day 14 (Fig. 3a) and which is due to the increase in the size of the structures. Cell death seems to affect mainly cells that are already differentiated and secrete collagen or that are already in an advanced stage of differentiation, while those that are still undifferentiated are affected somewhat less. This hypothesis is supported by the analysis of the expression of the stemness markers NANOG and OCT4 (Fig. 5d-e). A key aspect of hMSCs for therapeutic applications is their degree of stemness and their multilineage differentiation capabilities. The expression of the pluripotency markers OCT4 and NANOG has been described to influence deeply the self-renewal and undifferentiated state thereof [46]. In vitro 2D cultures of MSCs reduce their capacity for self-renewal and multipotency, which can be improved by 3D culture methods, especially as these systems are able to recapitulate physiological stem cell niches [47,48]. OCT-4 and NANOG were significantly upregulated in CTL-spheroids compared to cells in MF-spheroids. The self-renewal markers of both types of hMSC spheroids showed a time-dependent increase, but CTL-spheroids exhibited at day 4 a 12- and 9-fold increase in gene expression of NANOG and OCT4, respectively, while an average 2-fold increase was observed in MF-spheroids. Thus, it cannot be ruled out that the improved chondrogenic differentiation abilities of CTL-spheroids are also due to an improvement in their differentiation abilities. In the CTL-spheroids, the expression level increased from day 7 to day 21, from ~ 30 to ~2300 and ~1700-fold for NANOG and OCT4, respectively (Fig. 5d-e). This massive increase in expression alongside with the downregulation of COL2A1 might be attributed to the presence of cellular heterogeneity within the spheroids, i.e., populations of cells that are asynchronous in the differentiation process, as previously suggested. Cell death seems to affect mainly already differentiated cells in the central part of the structures, and TEM images of CTL-spheroids in these regions at day 14 show a partially degraded cell matrix associated with the presence of necrotic cells (Fig. 8). The cell population is then enriched with as yet undifferentiated cells, most likely concentrated on the outer surface of the spheroids, as indicated by the TEM images. The delayed differentiation of this cell population could potentially account for the second peak of COL2A1 expression observed at day 21. At variance, in MF-spheroids the absence of CTL matrix results in the deposition of few collagen fibers with no banding organization, suggesting that CTL in spheroids has a role in stimulating the deposition of mature collagen (Fig. 9).

## 5. Conclusions

The ability of lactose-modified chitosan to promote cell aggregation, particularly in primary cells, is well known. In the present work, given the bioactive properties of this polysaccharide, we investigated its effects on hMSC spheroid formation, its interaction with cells, and its ability to affect cell viability and chondrogenic differentiation compared to MF-spheroids. A 3D-cell culture platform was constructed by coating a culture plate with the functional polymer. Assembly into spheroids occurs spontaneously and appears to be related to and driven by CTL and its close molecular interaction with cells to form an active, natural ECM-like network for the neighboring cells.

The experimental data highlight not only the substantial enhancement of stemness and pro-chondrogenic properties in CTL-spheroids compared to the control group but also, more importantly, the acceleration of the differentiation process by a minimum of two weeks when compared to spheroids grown through conventional methods.

The use of CTL to form spheroids increases viability and promotes chondrogenic differentiation and matrix deposition in a very short time frame, which, in terms of in vivo application, allows earlier implantation of living and differentiated structures, thus avoiding potentially detrimental effects due to dead cells on the overall outcome of cartilage regeneration. In the field of biomaterials, recapitulation of stem cell niches by developing microenvironments with physiologically similar niche properties that act on stem cell regulatory mechanisms to harness their regenerative capacity is a key issue. From this point of view, the use of lactose-modified chitosan as a basis for generating spheroids represents a versatile, straightforward, and functionally advantageous technological platform for applications in stem cell-based tissue engineering and regenerative medicine. Such an approach has the potential to enhance the therapeutic effectiveness of hMSCs. Future studies will be aimed at identifying the molecular and/or biomechanical factors underlying the observed biological response and activate specific signaling pathways that may regulate cell biology as it occurs in vivo.

## CRediT authorship contribution statement

**F. Scognamiglio:** Writing – review & editing, Writing – original draft, Investigation, Conceptualization. **C. Pizzolitto:** Writing – review & editing, Investigation, Conceptualization. **M. Romano:** Writing – review & editing, Investigation. **G. Teti:** Writing – review & editing, Investigation. **S. Zara:** Writing – review & editing, Investigation. **M. Conz:** Writing – review & editing, Investigation. **I. Donati:** Writing – review & editing, Conceptualization. **D. Porrelli:** Writing – review & editing, Investigation. **M. Falconi:** Writing – review & editing. **E. Marsich:** Writing – review & editing, Writing – original draft, Supervision, Conceptualization.

## Declaration of competing interest

The authors declare that they have no known competing financial interests or personal relationships that could have appeared to influence the work reported in this paper.

## Data availability

Data will be made available on request.

## Acknowledgments

This research did not receive any specific grant from funding agencies in the public, commercial, or not-for-profit sectors.

## References

[1] J.C. Bernhard, G. Vunjak-Novakovic, Should we use cells, biomaterials, or tissue engineering for cartilage regeneration? Stem Cell Res Ther 7 (2016) 56, https://doi.org/10.1186/s13287-016-0314-3.
[2] R. Karuppal, Current concepts in the articular cartilage repair and regeneration, J. Orthop. 14 (2017) A1–A3, https://doi.org/10.1016/j.jor.2017.05.001.
[3] E.V. Medvedeva, E.A. Grebenik, S.N. Gornostaeva, V.I. Telpuhov, A.V. Lychagin, P. S. Timashev, A.S. Chagin, Repair of damaged articular cartilage: current approaches and future directions, Int. J. Mol. Sci. 19 (2018) 2366, https://doi.org/10.3390/ijms19082366.
[4] A. Mobasheri, G. Kalamegam, G. Musumeci, M.E. Batt, Chondrocyte and mesenchymal stem cell-based therapies for cartilage repair in osteoarthritis and related orthopaedic conditions, Maturitas 78 (2014) 188–198, https://doi.org/10.1016/j.maturitas.2014.04.017.
[5] M.F. Pittenger, A.M. Mackay, S.C. Beck, R.K. Jaiswal, R. Douglas, J.D. Mosca, M. A. Moorman, D.W. Simonetti, S. Craig, D.R. Marshak, Multilineage potential of

adult human mesenchymal stem cells, Science 284 (1999) 143–147, https://doi.org/10.1126/science.284.5411.143.
[6] F. Staubli, M.J. Stoddart, M. D'Este, A. Schwab, Pre-culture of human mesenchymal stromal cells in spheroids facilitates chondrogenesis at a low total cell count upon embedding in biomaterials to generate cartilage microtissues, Acta Biomater. 143 (2022) 253–265, https://doi.org/10.1016/j.actbio.2022.02.038.
[7] J.-Y. Ko, E. Lee, J.-W. Park, J. Kim, G.-I. Im, Enhancement of cartilage regeneration efficiency with human adipose stem cell three dimensional spheroid, Osteoarthr. Cartil. 28 (2020) S515–S516, https://doi.org/10.1016/j.joca.2020.02.809.
[8] A.V. Tsvetkova, I.V. Vakhrushev, Yu.B. Basok, A.M. Grigor'ev, L.A. Kirsanova, A. Yu Lupatov, V.I. Sevastianov, K.N. Yarygin, Chondrogeneic potential of MSC from different sources in spheroid culture, Bull. Exp. Biol. Med. 170 (2021) 528–536, https://doi.org/10.1007/s10517-021-05101-x.
[9] J.B. do Amaral, P. Rezende-Teixeira, V.M. Freitas, G.M. Machado-Santelli, MCF-7 cells as a three-dimensional model for the study of human breast cancer, Tissue Eng. Part C Methods 17 (2011) 1097–1107, https://doi.org/10.1089/ten.tec.2011.0260.
[10] J. Lee, G.D. Lilly, R.C. Doty, P. Podsiadlo, N.A. Kotov, In vitro toxicity testing of nanoparticles in 3D cell culture, Small 5 (2009) 1213–1221, https://doi.org/10.1002/smll.200801788.
[11] K. Białkowska, P. Komorowski, M. Bryszewska, K. Miłowska, Spheroids as a type of three-dimensional cell cultures-examples of methods of preparation and the Most important application, Int. J. Mol. Sci. 21 (2020) E6225, https://doi.org/10.3390/ijms21176225.
[12] S.-F. Chen, Y.-C. Chang, S. Nieh, C.-L. Liu, C.-Y. Yang, Y.-S. Lin, Nonadhesive culture system as a model of rapid sphere formation with cancer stem cell properties, PLoS One 7 (2012) e31864, https://doi.org/10.1371/journal.pone.0031864.
[13] G.-S. Huang, L.-G. Dai, B.L. Yen, S. Hsu, Spheroid formation of mesenchymal stem cells on chitosan and chitosan-hyaluronan membranes, Biomaterials 32 (2011) 6929–6945, https://doi.org/10.1016/j.biomaterials.2011.05.092.
[14] S.-J. Lin, S.-H. Jee, W.-C. Hsaio, S.-J. Lee, T.-H. Young, Formation of melanocyte spheroids on the chitosan-coated surface, Biomaterials 26 (2005) 1413–1422, https://doi.org/10.1016/j.biomaterials.2004.05.002.
[15] P. Verma, V. Verma, P. Ray, A.R. Ray, Formation and characterization of three dimensional human hepatocyte cell line spheroids on chitosan matrix for in vitro tissue engineering applications, In Vitro Cell.Dev.Biol.-Animal 43 (2007) 328–337, https://doi.org/10.1007/s11626-007-9045-1.
[16] C. Pizzolitto, F. Esposito, P. Sacco, E. Marsich, V. Gargiulo, E. Bedini, I. Donati, Sulfated lactose-modified chitosan, A novel synthetic glycosaminoglycan-like polysaccharide inducing chondrocyte aggregation, Carbohydr. Polym. 288 (2022) 119379, https://doi.org/10.1016/j.carbpol.2022.119379.
[17] C. Pizzolitto, F. Scognamiglio, G. Baldini, R. Bortul, G. Turco, I. Donati, V. Nicolin, E. Marsich, Bioactive lactose-modified chitosan acts as a temporary extracellular matrix for the formation of chondro-aggregates, ACS Appl. Polym. Mater. 5 (2023) 504–516, https://doi.org/10.1021/acsapm.2c01613.
[18] E. Marsich, M. Borgogna, I. Donati, P. Mozetic, B.L. Strand, S.G. Salvador, F. Vittur, S. Paoletti, Alginate/lactose-modified chitosan hydrogels: a bioactive biomaterial for chondrocyte encapsulation, J. Biomed. Mater. Res. A 84A (2008) 364–376, https://doi.org/10.1002/jbm.a.31307.
[19] F. Scognamiglio, A. Travan, I. Donati, M. Borgogna, E. Marsich, A hydrogel system based on a lactose-modified chitosan for viscosupplementation in osteoarthritis, Carbohydr. Polym. 248 (2020) 116787, https://doi.org/10.1016/j.carbpol.2020.116787.
[20] E. Tarricone, E. Mattiuzzo, E. Belluzzi, R. Elia, A. Benetti, R. Venerando, V. Vindigni, P. Ruggieri, P. Brun, Anti-inflammatory performance of lactose-modified chitosan and hyaluronic acid mixtures in an in vitro macrophage-mediated inflammation osteoarthritis model, Cells 9 (2020) 1328, https://doi.org/10.3390/cells9061328.
[21] I. Donati, S. Stredanska, G. Silvestrini, A. Vetere, P. Marcon, E. Marsich, P. Mozetic, A. Gamini, S. Paoletti, F. Vittur, The aggregation of pig articular chondrocyte and synthesis of extracellular matrix by a lactose-modified chitosan, Biomaterials 26 (2005) 987–998, https://doi.org/10.1016/j.biomaterials.2004.04.015.
[22] F. Scognamiglio, A. Travan, M. Borgogna, I. Donati, E. Marsich, Development of biodegradable membranes for the delivery of a bioactive chitosan-derivative on cartilage defects: a preliminary investigation, J. Biomed. Mater. Res. A 108 (2020) 1534–1545, https://doi.org/10.1002/jbm.a.36924.
[23] P. Sacco, F. Furlani, A. Marfoglia, M. Cok, C. Pizzolitto, E. Marsich, I. Donati, Temporary/permanent dual cross-link gels formed of a bioactive lactose-modified chitosan, Macromol. Biosci. 20 (2020) 2000236, https://doi.org/10.1002/mabi.202000236.
[24] K.J. Livak, T.D. Schmittgen, Analysis of relative gene expression data using real-time quantitative PCR and the 2(-Delta Delta C(T)) method, Methods 25 (2001) 402–408, https://doi.org/10.1006/meth.2001.1262.
[25] Y. Mao, T. Hoffman, A. Wu, J. Kohn, An innovative laboratory procedure to expand chondrocytes with reduced dedifferentiation, Cartilage 9 (2018) 202–211, https://doi.org/10.1177/1947603517746724.
[26] J.A.M. Steele, S.D. McCullen, A. Callanan, H. Autefage, M.A. Accardi, D. Dini, M. M. Stevens, Combinatorial scaffold morphologies for zonal articular cartilage engineering, Acta Biomater. 10 (2014) 2065–2075, https://doi.org/10.1016/j.actbio.2013.12.030.
[27] M. Barisam, M.S. Saidi, N. Kashaninejad, N.-T. Nguyen, Prediction of necrotic Core and hypoxic zone of multicellular spheroids in a microbioreactor with a U-shaped barrier, Micromachines 9 (2018) 94, https://doi.org/10.3390/mi9030094.
[28] R. Coyle, J. Yao, D. Richards, Y. Mei, The effects of metabolic substrate availability on human adipose-derived stem cell spheroid survival, Tissue Eng. Part A 25 (2019) 620–631, https://doi.org/10.1089/ten.tea.2018.0163.
[29] S. Däster, N. Amatruda, D. Calabrese, R. Ivanek, E. Turrini, R.A. Droeser, P. Zajac, C. Fimognari, G.C. Spagnoli, G. Iezzi, V. Mele, M.G. Muraro, Induction of hypoxia and necrosis in multicellular tumor spheroids is associated with resistance to chemotherapy treatment, Oncotarget 8 (2016) 1725–1736, https://doi.org/10.18632/oncotarget.13857.
[30] K. Niibe, Y. Ohori-Morita, M. Zhang, Y. Mabuchi, Y. Matsuzaki, H. Egusa, A shaking-culture method for generating bone marrow derived mesenchymal stromal/stem cell-spheroids with enhanced multipotency in vitro, Front. Bioeng. Biotechnol. 8 (2020), https://doi.org/10.3389/fbioe.2020.590332.
[31] M.C. Decarli, A. Seijas-Gamardo, F.L.C. Morgan, P. Wieringa, M.B. Baker, J.V.L. Silva, Â.M. Moraes, L. Moroni, C. Mota, Bioprinting of stem cell spheroids followed by post-printing chondrogenic differentiation for cartilage tissue engineering, Advanced Healthcare Materials n/a (n.d.) 2203021. doi:https://doi.org/10.1002/adhm.202203021.
[32] V. Lefebvre, M. Dvir-Ginzberg, SOX9 and the many facets of its regulation in the chondrocyte lineage, Connect. Tissue Res. 58 (2017) 2–14, https://doi.org/10.1080/03008207.2016.1183667.
[33] S.R. Herlofsen, A.M. Küchler, J.E. Melvik, J.E. Brinchmann, Chondrogenic differentiation of human bone marrow-derived mesenchymal stem cells in self-gelling alginate discs reveals novel chondrogenic signature gene clusters, Tissue Eng. Part A 17 (2011) 1003–1013, https://doi.org/10.1089/ten.TEA.2010.0499.
[34] Y. Mao, T. Block, A. Singh-Varma, A. Sheldrake, R. Leeth, S. Griffey, J. Kohn, Extracellular matrix derived from chondrocytes promotes rapid expansion of human primary chondrocytes in vitro with reduced dedifferentiation, Acta Biomater. 85 (2019) 75–83, https://doi.org/10.1016/j.actbio.2018.12.006.
[35] I.-C. Lin, T.-J. Wang, C.-L. Wu, D.-H. Lu, Y.-R. Chen, K.-C. Yang, Chitosan-cartilage extracellular matrix hybrid scaffold induces chondrogenic differentiation to adipose-derived stem cells, regenerative, Therapy 14 (2020) 238–244, https://doi.org/10.1016/j.reth.2020.03.014.
[36] S. Li, The basic characteristics of extracellular vesicles and their potential application in bone sarcomas, J. Nanobiotechnol. 19 (2021) 277, https://doi.org/10.1186/s12951-021-01028-7.
[37] S. Li, J. Liu, S. Liu, W. Jiao, X. Wang, Chitosan oligosaccharides packaged into rat adipose mesenchymal stem cells-derived extracellular vesicles facilitating cartilage injury repair and alleviating osteoarthritis, J. Nanobiotechnol. 19 (2021) 343, https://doi.org/10.1186/s12951-021-01086-x.
[38] S. Li, J. Liu, S. Liu, W. Jiao, X. Wang, Mesenchymal stem cell-derived extracellular vesicles prevent the development of osteoarthritis via the circHIPK3/miR-124-3p/MYH9 axis, J. Nanobiotechnol. 19 (2021) 194, https://doi.org/10.1186/s12951-021-00940-2.
[39] T. Gonzalez-Fernandez, A.J. Tenorio, A.M. Saiz Jr., J.K. Leach, Engineered cell-secreted extracellular matrix modulates cell spheroid Mechanosensing and amplifies their response to inductive cues for the formation of mineralized tissues, Adv. Healthc. Mater. 11 (2022) 2102337, https://doi.org/10.1002/adhm.202102337.
[40] S.J. Yu, G. Choi, Y. Cho, M. Lee, Y. Cho, J.H. Shin, E. Lee, S.G. Im, Three-dimensional spheroid culture on polymer-coated surface potentiate stem cell functions via enhanced cell–extracellular matrix interactions, ACS Biomater Sci. Eng. 6 (2020) 2240–2250, https://doi.org/10.1021/acsbiomaterials.9b01738.
[41] J. Park, Y.S. Kim, S. Ryu, W.S. Kang, S. Park, J. Han, H.C. Jeong, B.H. Hong, Y. Ahn, B.-S. Kim, Graphene potentiates the myocardial repair efficacy of mesenchymal stem cells by stimulating the expression of angiogenic growth factors and gap junction protein, Adv. Funct. Mater. 25 (2015) 2590–2600, https://doi.org/10.1002/adfm.201500365.
[42] K.C. Murphy, B.P. Hung, S. Browne-Bourne, D. Zhou, J. Yeung, D.C. Genetos, J. K. Leach, Measurement of oxygen tension within mesenchymal stem cell spheroids, J. R. Soc. Interface 14 (2017) 20160851, https://doi.org/10.1098/rsif.2016.0851.
[43] L.-W. Hsu, P.-L. Lee, C.-T. Chen, F.-L. Mi, J.-H. Juang, S.-M. Hwang, Y.-C. Ho, H.-W. Sung, Elucidating the signaling mechanism of an epithelial tight-junction opening induced by chitosan, Biomaterials 33 (2012) 6254–6263, https://doi.org/10.1016/j.biomaterials.2012.05.013.
[44] L.-W. Hsu, Y.-C. Ho, E.-Y. Chuang, C.-T. Chen, J.-H. Juang, F.-Y. Su, S.-M. Hwang, H.-W. Sung, Effects of pH on molecular mechanisms of chitosan–integrin interactions and resulting tight-junction disruptions, Biomaterials 34 (2013) 784–793, https://doi.org/10.1016/j.biomaterials.2012.09.082.
[45] A.J. Morwood, I.A. El-Karim, S.A. Clarke, F.T. Lundy, The role of extracellular matrix (ECM) adhesion motifs in functionalised hydrogels, Molecules 28 (2023) 4616, https://doi.org/10.3390/molecules28124616.
[46] E. Pierantozzi, B. Gava, I. Manini, F. Roviello, G. Marotta, M. Chiavarelli, V. Sorrentino, Pluripotency regulators in human mesenchymal stem cells: expression of NANOG but not of OCT-4 and SOX-2, Stem Cells Dev. 20 (2011) 915–923, https://doi.org/10.1089/scd.2010.0353.
[47] P. Rybkowska, K. Radoszkiewicz, M. Kawalec, D. Dymkowska, B. Zabłocka, K. Zabłocki, A. Sarnowska, The metabolic changes between monolayer (2D) and three-dimensional (3D) culture conditions in human mesenchymal stem/stromal cells derived from adipose tissue, Cells 12 (2023) 178, https://doi.org/10.3390/cells12010178.
[48] X. Wu, J. Su, J. Wei, N. Jiang, X. Ge, Recent advances in three-dimensional stem cell culture systems and applications, Stem Cells Int. 2021 (2021) 9477332, https://doi.org/10.1155/2021/9477332.